Nuclear Engineering and Technology 56 (2024) 477–484

Contents lists available at ScienceDirect

Nuclear Engineering and Technology

journal homepage: www.elsevier.com/locate/net

Original Article

Characterization and experimental investigation for gamma–ray shielding competence of basalt-doped polyethylene nanocomposites

I.A. El-Mesady [a], F.I. El-Agawany [a,*], H. El-Samman [a], Y.S. Rammah [a], A. Hussein [a], R.A. Elsad [b]

[a] Physics Department, Menoufia University, 32511, Shebin El Koom, Egypt
[b] Basic Engineering Science Department, Menoufia University, 32511, Shebin El-Koom, Egypt

ARTICLE INFO

Keywords:
FTIR
HPGe detector
Dielectric constant
Transmission factor

ABSTRACT

Experimental investigations on gamma - rays attenuation parameters and dielectric spectroscopic properties were done on a polymeric mixture with chemical composition (100-x) polyethylene + x basalt, where x = 0, 1, 3, 5, 10, and 20 wt%. Using the melting blending technique,six nanocomposite polymeric samples were prepared. The linear attenuation coefficient μ of each prepared set of samples was measured using a gamma-ray spectrometer including High Purity Germanium detector (HPGe) at energies 662.5, 1173.24, and 1332.51 keV. Based on the measured values of (μ) and sample density, the other effective shielding parameters were calculated. the values of μ showed an increase with increasing the dopant ratios from 0.0 up to 20.0 wt%. In addition, the μ values decreased with the photon's energy. The μ values were found 0.0847 up to 0.1175 cm^{-1}, 0.0571 up to 0.0855 cm^{-1}, and 0.0543 up to 0.075 cm^{-1} at 662.5, 1173.24, and 1332.51 keV. for B0 up to B20, respectively. The ATR spectroscopy was done on the prepared samples, and a good evidence of adding the filler to the pure polyethylene (HDPE) was obtained. Besides, an enhancement in dielectric constant by insertion of basalt NPs also recorded and can be attributed to the large dielectric constant of basalt compared to pure HDPE.

1. Introduction

We live in an environment that is not free of radiation, and this radiation is considered a double-edged sword because it is considered one of the sources used in various applications as long as it is directed for peaceful use. On the contrary, it can be used in non-peaceful uses, and here lies its danger, which increases this risk because this radiation is not visible to the naked eye. X- and gamma–rays are found among the different types of radiation. These two types are uncharged, mass-less, and highly penetrating ionizing radiations [1,2]. These types of radiations and the charged ionizing ones are used in different applications in our daily life as agriculture, medical science, research, industry, ecology, ….etc. [3–5]. Protection from ionizing radiation is essential, and three important factors affecting the protection process are distance, time, and the shielding materials [6,7]. The choice of shielding materials is crucial and different materials nowadays have been prepared to be a shield for incident gammas instead of the superior lead due to some limitations [8]. These materials include glasses, glass ceramics, alloys, concretes, and polymers [9–18]. One must select suitable materials with high atomic numbers and density to prevent hazards from gamma rays. In this regard, some researchers prepared different materials based on polymers doped with high-density modifiers to be examined as shielding materials. Addition of these modifiers to the host polymers enhances their optical, magnetic, and dielectric properties [3,4,9–18].

Basalt rocks have been used because of the tremendous advantages that make them able to improve the properties of the materials added to them. One of the most important advantages is its density of about 3 g per cm^3, improving the shield's properties against ionizing rays. This rock is strongly available in Egypt, so it was resorted to using it in this work [3,4].

This study's main objective is to perform an experimental investigation to examine the shielding effectiveness of the prepared (100-x) polyethylene + x basalt, where x = 0, 1, 3, 5, 10, and 20 wt%. The shielding examination was done via the linear attenuation coefficient (μ) measurements obtained from the photon transmission intensities using a high-resolution HPGe detector at 662.5, 1173.24, and 1332.51 keV.. The other shielding parameters, including the mass attenuation coefficient (m), half-value layer (HVL), transmission factor (TF%), radiation protection efficiency (RPE%), and buildup factors (EBF, EABF), were also calculated based on the sample thickness (x) and densities (ρ). In

* Corresponding author.
E-mail address: fouad.ismail520@science.menofia.edu.eg (F.I. El-Agawany).

https://doi.org/10.1016/j.net.2023.10.023
Received 19 August 2023; Received in revised form 9 October 2023; Accepted 17 October 2023
Available online 23 October 2023

addition, the prepared polymers' structural characterization has been investigated through attenuation total reflection spectroscopy (ATR). Finally, the dielectric spectroscopy of the prepared polymers has been investigated via the dielectric constant (ε′) and loss tangent (tan δ) measurements.

2. Experimental procedure

2.1. Preparation methodology

Six nanocomposite polymeric sets of samples coded as B0, B1, B3, B5, B10, and B20 with the chemical composition (100-x) polyethylene + x basalt, where x = 0, 1, 3, 5, 10, and 20 wt % were prepared by the melt blending technique [3]. Each set consists of 6 homogeneous sheets of different thicknesses. The sample density was measured at room temperature (RT) relying on Archimedes' principle. The chemical composition of the filler (basalt) was investigated using X–ray fluorescence (XRF) technique as parts per million (ppm) and presented in Table 1.

2.2. Characterization techniques

ATR of the prepared samples was measured via a spectrometer Burker in the wavenumber range 4000–400 cm^{-1} at RT. Using HIOKI 3532-50 LCR Hi-tester equipment with a constant applied voltage of 1 V across a frequency range of 50 Hz to 5 MHz, dielectric spectroscopic measurements of the B0–B20 nanocomposites sheets were performed. Before being inserted between two electrodes under the fixed stress produced by the spring, the examined B0 – B20 nanocomposites with a diameter of 2 cm were covered at both faces with a thin layer of silver. Using the software LabVIEW, the measured capacitance (C) and resistance (R) of the B0 – B20 nanocomposites under investigation were recorded 14 times at each applied field frequency.

The dielectric constant (ε′) and the loss tangent (tan δ) are calculated using the following equations:

$$\varepsilon' = \frac{d \cdot c}{\varepsilon_0 \cdot A} \quad (1)$$

$$\tan\delta = \frac{1}{2\pi f R C} \quad (2)$$

Where ε_0 d, A, and f are the free space permittivity, the sample thickness, the small electrode's cross-section area, and the applied field frequency, respectively.

2.3. Gamma–ray shielding using HPGe detector

The prepared samples were examined using a collimated beam of gamma photons from Cs-137- and Co-60-point sources which were fixed at 10 cm for the centre of the gamma rays' detector. The gamma radiation attenuation properties of the synthesized polymer composites. In the present study, the used gamma-ray spectrometer consists of a 60 % relative efficiency hyper pure germanium detector (HPGe) connected to an electric cooling system. The detector has a resolution (FWHM) of 1.9 keV at 1332 keV γ-ray line of ^{60}Co. The detector is connected to a digital spectrometer DSPC-pro which has a high voltage, advanced spectroscopy amplifier, and 8 k multichannel analyzer. The prepared samples were introduced between the gamma source and the detector in a such way that covered the entrance window of the detector. Each thickness of the sample was counted for 15 min live time. The net area under the photo peak of 662.5, 1173.24, and 1332.51 keV. were estimated and used to calculate the linear attenuation coefficient μ. The advantage of a gamma spectrometer with a HPGe detector over a NaI spectrometer lies in the high resolution which makes Germanium unique for distinguishing between photopeak and Compton scattering plateau of the same photons.

3. Results and discussion

3.1. Morphology of the prepared samples

Table 1 presents the elemental composition of the basalt filler added to the pure HDPE. As obtained by XRF spectroscopy, SiO_2 is the most prevalent constituent of basalt with 49.96 wt %. Besides, the other oxides forming basalt are Al_2O_3, CaO, FeO, Fe_2O_3, and MgO. To show if these oxides are contained in the composed mixture or not, EDX analysis was also performed on B0, B5, and B20 nanocomposite polymeric samples. The obtained data from EDX are presented in Table 2 and refer to that for B0 (100 wt % HDPE, $(C_2H_4)_n$, so only C is prevalent. For B5 and B20, the C ratio decreased as the HDPE decreased, and one noticed that Si, Al, Ca, Fe, Mg, etc., were contained in both samples with increasing ratios moving from B5 to B20. These results ensure that basalt is successfully modified in the polymer matrix. To study the morphology of the prepared B0, B5, and B20 samples, the scanning electron microscopy (SEM) was performed and presented in Fig. 1a, b, and c. As presented in Fig. 1a, homogeneous sheets showed that HDPE is clear as in B0. The presence of basalt in the mixtures B5 and B20 samples was investigated where spherical particles were presented on the homogeneous surface in the B0 sample [19–21]. The densities of the spherical particles increased in B20 than in the B5 sample, which ensured the distribution of basalt into the mixture.

3.2. Attenuation total reflection spectroscopy (ATR)

The ATR spectra of pure HDPE (B0) and the modified nanocomposite B1 – B20 samples were done at RT and the transmittance of the samples versus wave number in cm^{-1} were presented in Fig. 2 in the 4000–400 cm^{-1}. The left-hand side of this Figure presented characteristic bands located in the region 3500–3800 cm^{-1} for the O–H bond stretching vibration associated with H_2O [22,23]. Other absorption peaks at 2914 cm^{-1} and 2844 cm^{-1} are considered symmetrical and asymmetric stretching vibrations of CH_2.

Also, at 1465 cm^{-1}, a presence of CH_2 bending; a typical band at 722 cm^{-1} represents CH_2 rocking was also presented [24–26].

It is seen that the four characteristic bands are found without any change in the peak positions for all prepared polymeric samples; B0 which is basalt free and also B1 – B20 with different ratios of basalt added as a modifier in the host material.

On the right-hand side of Fig. 2, the transmittance is plotted as a function of the wave number in the 700–400 cm^{-1} range. In this region, small shifts in the peak positions were noticed. Also, a decrease and increase in the peak intensities were noticed which may be attributed to the possible bond formation with the materials enhanced with basalt filler added to the pure HDPE.

3.3. Gamma-ray attenuation properties

The dependence of μ expressed in cm^{-1} on the basalt ratios, 0–20 wt %, is presented in Fig. 3. As seen, μ values possess a multiple character; firstly, it has higher values for the 662.5 keV than 1173.24 and 1332

Table 1
Chemical composition of basalt filler examined by XRF technique.

Oxides	SiO_2	TiO_2	Al_2O_3	Fe_2O_3	FeO	MnO	MgO	CaO	Na_2O	K_2O	P_2O_5
Composition, (wt%)	49.96	1.87	15.99	3.85	7.24	0.2	6.84	9.62	2.96	1.12	0.35

Table 2
EXD analysis for B0, B5, and B20 polymeric samples.

Sample	Elements detected by EDX, weight %											
	C	O	Na	Mg	Al	Si	P	K	Ca	Ti	Mn	Fe
B0	100	–	–	–	–	–	–	–	–	–	–	–
B5	72.6	25.57	0.03	0.09	0.38	0.65	0.05	0.1	0.16	0.01	0.06	0.3
B20	71.46	23.56	0.09	0.21	1.04	2.03	0.05	0.16	0.53	0.1	0.08	0.71

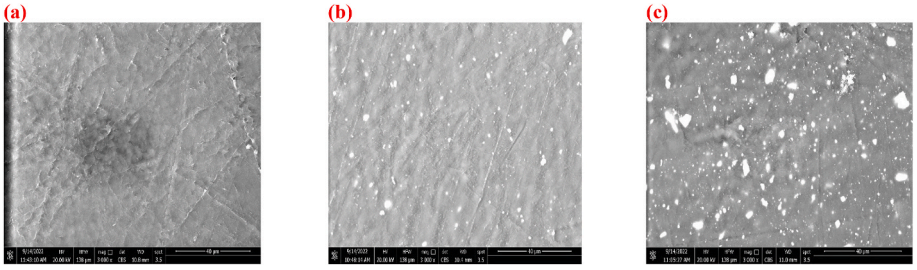

Fig. 1. SEM images of B0 (a), B5 (b), and B20 (c) nanocomposites.

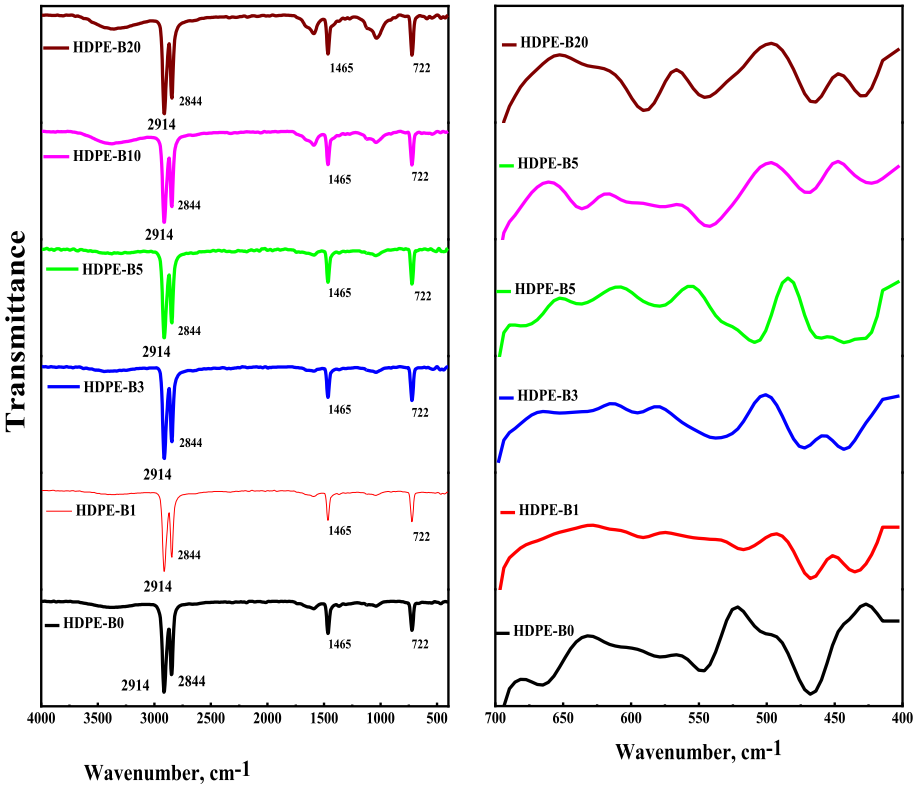

Fig. 2. ATR spectra for B0 – B20 nanocomposites at 4000–400 cm^{-1}.

keV. So, it was linearly decreased with increasing the gamma energies from 662 to 1332.51 keV. For 662.5 keV, the μ values were found 0.0847 up to 0.1175 cm^{-1}, 0.0571 up to 0.0855 cm^{-1} at 1173.24 keV, 0.0543 up to 0.075 cm^{-1} at 1332.51 keV for B0 up to B20, respectively. These measured values for the linear attenuation coefficient showed the other multiple characters that reflected the linear increase in the μ values with the increase in the filler concentration (basalt wt.%). The obtained linear decrements might be attributed to the Compton scattering (CS) interaction mechanism, which is most dominant in this studied energy zone. This behavior matches Fig. 4, which presented the μ values versus the photon energy in keV for B0 – B20 polymeric samples.

Regarding the density of the samples, the measured values revealed that the enhancement in the filler (basalt) weight percentage in the composite led to an increase in the density of the samples from 0.945 to 1.33 g/cm^3 due to the high molecular weight of basalt which approximately equal 70.85 g/mol which entered the composite as substitutional of polyethylene polymers with low molecular weight. This density enhancement also reflected the composite's shielding capacity.

The linear attenuation coefficient was also calculated theoretically and presented in Table 3. The experimental results were compared for measurement accuracy with the theoretical results calculated by the Phy-X/PSD program [27] and simulated by MCNP Monte Carlo code. The obtained results showed that the relative difference (RD%) at 662.5 keV ranged between 1.28 and 7.90 %, while at 1173.24 keV, RD ranged

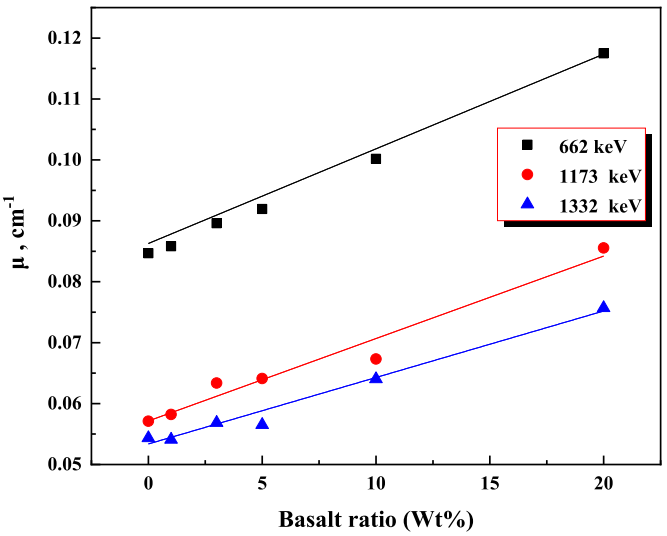

Fig. 3. μ values versus basalt ratio (Wt. %) at 662, 1173, and 1332 keV.

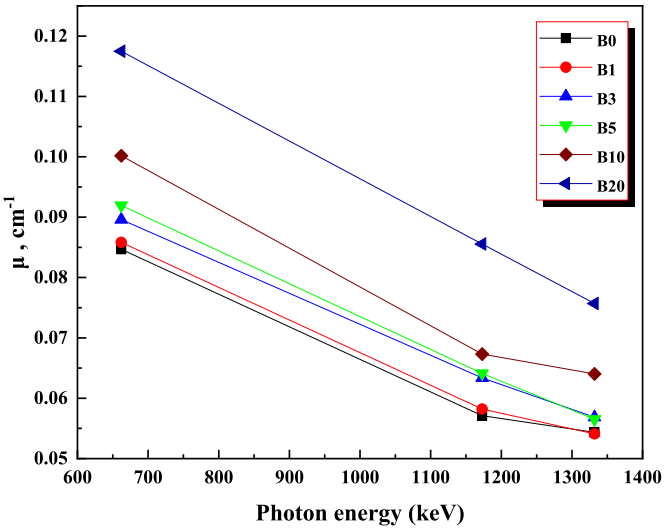

Fig. 4. μ values in cm^{-1} versus photon energy (keV) for B0 – B20 polymers.

from 0.4 to 10.55 %, and at 1332.51 keV, the RD ranged from 4.65 to 9.20 %. These small RD values reflected that the detection methodology for attenuation parameter measurements reached an acceptable degree.

It is preferable to translate this efficiency into how much distance or sample thickness can attenuate the incident gamma photons to investigate the shielding capacity of the investigated polymeric samples. To achieve this, the half–value layer (HVL) was determined from the μ values through the well-known relation; (HVL = 0.693/μ).

Like μ, HVL seems affected by both the prepared samples' chemical composition and the incident energies. The effect of adding the basalt filler with ratios ranging from 1 to 20 wt% to the polyethylene polymers on HVL at the three gamma energies 662.5, 1173.24, and 1332.51 keV was depicted in Fig. 5. This Figure introduced an inverse trend obtained in Fig. 3 regarding μ values. This reverse trend shows that HVL linearly decreased with increasing basalt in the polymer matrix. At the same time, it also increased with increasing the incident gammas. Results revealed that 8.1836 cm is sufficient to stop or attenuate 50 % of the intensity of the 662 keV radioisotope incident on HDPE (B0 sample).

In comparison, this value decreased linearly to 5.899 cm at adding 20 wt% of basalt forming B20 sample. For attenuating 50 % of the intensity of the Co-60 radioisotope, the sample thickness which seems to

Table 3
Experimental and theoretical linear attenuation coefficient of the prepared samples and the corresponding relative difference (RD%) at 662, 1173, and 1332 keV.

Sample	Density, g/cm^3	Energy, keV	Linear attenuation coefficient, μ (cm^{-1})		
			Exp.	MCNP	RD%
B0	0.945	662	0.0847	0.0831	1.90
		1173	0.0571	0.0632	9.72
		1332	0.0543	0.0593	8.32
B1	0.946	662	0.0858	0.0831	3.29
		1173	0.0582	0.0632	7.93
		1332	0.0541	0.0593	8.71
B3	0.953	662	0.0896	0.0836	7.18
		1173	0.0634	0.0636	0.40
		1332	0.0569	0.0596	4.65
B5	0.976	662	0.0919	0.0852	7.90
		1173	0.0641	0.0649	1.19
		1332	0.0565	0.0608	7.05
B10	1.14	662	0.1002	0.0989	1.28
		1173	0.0673	0.0753	10.55
		1332	0.0640	0.0705	9.20
B20	1.33	662	0.1175	0.1139	3.14
		1173	0.0855	0.0866	1.26
		1332	0.0757	0.0812	6.77

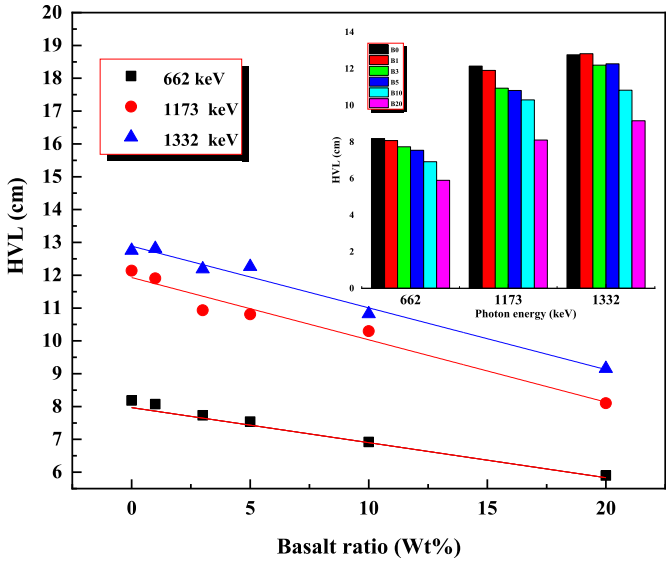

Fig. 5. HVL values versus basalt ratio (Wt. %) and input versus photon energy (keV) for B0 – B20 polymers at 662.5, 1173.24, and 1332.51 keV.

be sufficient is 12.1366 cm decreased to reach 8.1015 cm and 12.753 cm decreased to 9.1546 cm at 1173 and 1332 keV for B0 and B20, respectively. In conclusion, at the same energy, HVL decreased and increasing the photon energy overcame an increase.

Adding the filler with high concentrations in the fabricated polymeric samples increases the electron distribution inside the polymer matrix, which increases the cross-section probability, which means that the photon interaction probability with the prepared samples is also increased.

HVL and the other two parameters TVL and MFP were calculated based on the experimental results. These parameters are connected inversely with μ. Consequently, as presented in Table 4, HVL, TVL, and MFP of the B0 – B20 samples were calculated from experimental results at 662.5, 1173.24, and 1332.51 keV. B0 – B20 samples exhibit a hybrid trend; reduced with increasing the filler, despite being increased with

Table 4
HVL, TVL, MFP of the polymeric samples, and the ratio of HVL of the prepared samples to HVL of lead at 662, 1173, and 1332 keV.

Material	Energy, keV	HVL, *Cm*	TVL, cm	MFP, cm	HVL $_{Material}$/HVL $_{lead}$
Lead	662	0.5901	1.9610	0.8515	
	1173	1.0254	3.4076	1.4797	
	1332	1.1218	3.7280	1.6188	
B0	662	8.1836	27.1959	11.8089	13.8681
	1173	12.1366	40.3327	17.5131	11.8360
	1332	12.7530	42.3813	18.4026	11.3684
B1	662	8.0739	26.8314	11.6506	13.6822
	1173	11.9031	39.5569	17.1762	11.6083
	1332	12.8120	42.5772	18.4877	11.4209
B3	662	7.7340	25.7018	11.1601	13.1062
	1173	10.9340	36.3364	15.7778	10.6632
	1332	12.1878	40.5030	17.5871	10.8645
B5	662	7.5383	25.0516	10.8778	12.7746
	1173	10.8095	35.9226	15.5982	10.5418
	1332	12.2611	40.7466	17.6929	10.9299
B10	662	6.9184	22.9915	9.9833	11.7241
	1173	10.2956	34.2148	14.8566	10.0406
	1332	10.8231	35.9675	15.6177	9.6479
B20	662	5.8990	19.6038	8.5123	9.9967
	1173	8.1015	26.9231	11.6904	7.9008
	1332	9.1546	30.4227	13.2100	8.1606

increasing the incident photon energy.

Being an optimum and superior shielding material against incident gammas, the $\frac{HVL_{Material}}{HVL_{Lead}}$ ratio was also calculated at 662, 1173, and 1332 keV to define what extent the prepared materials can shield the incident gammas compared to lead [6]. This ratio was calculated at the three gamma energies led to the results presented in Table 4. For B0 at 662 keV, this ratio gave 13.8681, this means that HVL of the B0 is 13.86 times the HVL of lead. At 1173, this ratio became 11.3. For B5 sample, the HVL of the prepared material was 12.7, 10.54, and 10.9 times lead at 662, 1173, and 1332 keV, respectively. B20 ratio revealed that 5.89, 8.10, and 9.15 cm are equivalent to 0.59, 1.02, and 1.12 cm of lead leading to the HVL of the prepared samples was 9.99, 7.9, and 8.16 times lead. These obtained results show the advantages of adding 20 wt % of basalt to HDPE to enhance their shielding characteristics against gamma – rays.

The radiation protection efficiency (RPE) parameter, which indicated the ability of the investigated polymeric B0 – B20 materials to be an effective gamma shield through the measurements of the amount of energy deposited inside the polymer thickness, also calculated from the measured photon intensities I and I_0 which are the intensity of the photon beam after and before passing the prepared materials through the following relation:

$$\mathrm{RPE}(\%) = \left(1 - \frac{I}{I_0}\right) \mathrm{x}100 \tag{3}$$

RPE for the prepared samples was calculated for all samples at the three studied energies and different polymer thicknesses. Fig. S1 (supplementary materials) presented the RPE% versus sample thicknesses. It is more obvious from the Figure that the RPE increased linearly with increasing the sample thickness. Moreover, the RPE increases with increasing the filler concentration in the polymer matrix. The shielding efficiency of the prepared samples increased as much energy was deposited inside the polymers.

In addition, similarly to μ, the RPE was plotted against the basalt ratio at the studied energies 662.5, 1173.24, and 1332.51 keV and presented in Fig. 6. This Figure revealed that the less the photon energy, the more the RPE and vice versa. As the photon energy increased, the RPE decreased, while an overall increase in the RPE was noticed as the basalt ratio increased from 0.0 to 20 wt%.

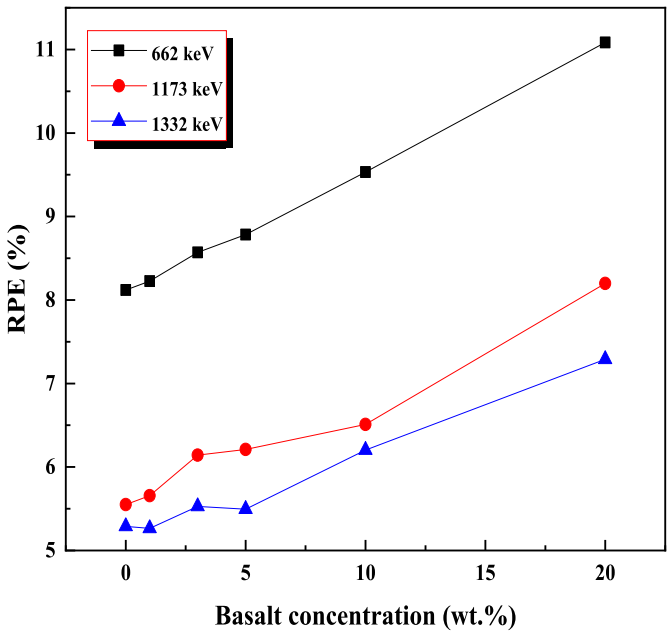

Fig. 6. RPE % of 1 cm sample thickness at 662, 1173, and 1332 keV.

The well-known beer–Lambert law which describes the incidence, absorbance, and transmission process when a beam hits a material of thickness t, is presented through the following relation;

$$I_0 e^{-\mu t} = I \tag{4}$$

Based on this law, it is easy to calculate the transmission factor TF% (I/I_0), a measure of the photons that can penetrate the thickness of the investigated shielding material.

The TF% is also calculated at the same thickness for all B0 – B20 polymers and presented in Fig. S2 (supplementary materials). This Figure assured that the thicker the polymers, the less the TF, as the photons make many collisions along their track length. So, it overcomes a high resistance leading to a decrease in the TF.

Fig. 7 shows the prepared polymers' TF at 1 cm thickness at 662.5, 1173.24, and 1332.51 keV. This Figure shows that the TF decreased with

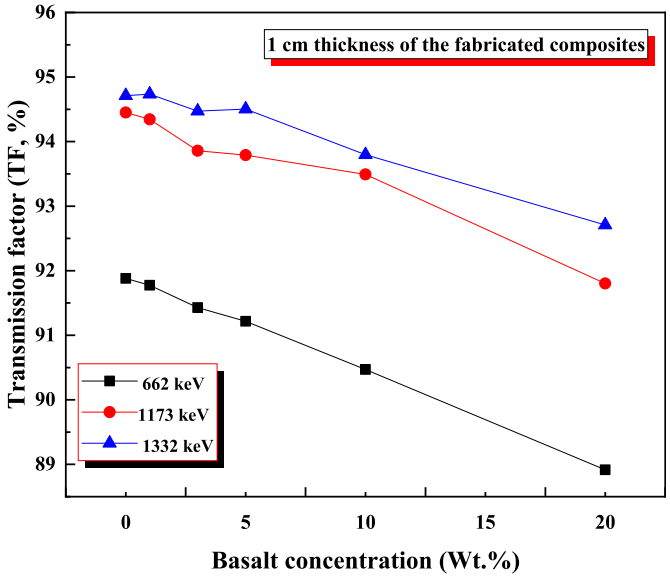

Fig. 7. Transmission factor TF% of 1 cm sample thickness at 662, 1173, and 1332 keV.

the filler enhancement and increased with increasing the incident gammas. The TF decreased from 92 % to 88 %, 94.44 %–91.8 %, and 94.71 %–92.7 % at 662.5, 1173.24, and 1332.51 keV, respectively. The increase in the TF trend is related to gamma photons' penetration power, that proportional to the photon energy. The buildup factor calculations determined the accumulated photons inside the prepared B0 – B20 polymeric samples. The EBF and EABF were calculated with the online software version of the Phy-X/PSD program and presented in Figs. S3–S5 (see supplementary materials).

The prepared B0 –B20 polymers presented in this study were compared to many investigated polymers in literature by (Atta et al., 2015), (Sharma et al., 2020), (Mahmoud et al., 2018a, b) (Akman et al., 2020), (Li et al., 2017), and (Abdo et al., 2003), [28–34]. The measured experimental mass attenuation coefficient of our prepared samples seemed to be suitable for gamma - ray shielding compared to other prepared materials in literature as styrene butadiene rubber, polyester concrete doped bismuth oxychloride, high density polyethylene doped and with out 50 % lead oxide nano filler, polyester doped lead iodide, basalt fiber with and without erbium oxide, and fiber plastic with and with out lead. The obtained values were presented in Table S1 and introduced B0 – B20 as a good gamma – ray shield among the polymers in literature.

3.4. Dielectric spectroscopic studies

Fig. 8 illustrates the dependence of the dielectric constant, ε', of B0 – B20 nanocomposites on applied field frequency at RT. It can be distinctly seen from Fig. 8 that the dependence of the dielectric constant, ε', of B0 – B20 nanocomposite samples takes a usual trend with an increase in the applied frequency in which the dielectric constant (ε') dramatically decreases in the low-frequency range and becomes almost constant in the high-frequency range. The noticed reduction in dielectric constant during a small frequency range can be assigned to reducing the orientation polarization contribution with frequency increasing [35–37]. The effective dielectric permittivity value is determined by the number of orientable dipoles and their ability to orient with field direction. More specifically, the free functional group dipoles in B0 – B20 nanocomposites do not have sufficient time at high frequency to align with the applied field direction.

Fig. 9 displays the effect of basalt NPs addition to the HDPE matrix on the dielectric constant at different frequencies 100,400, 1000 kHz. It is clear from plotted curves that the values of ε' are generally increased with an increase in the basalt NPs filler concentration. Nanocomposites' dielectric constant depends on their components' dielectric constant and

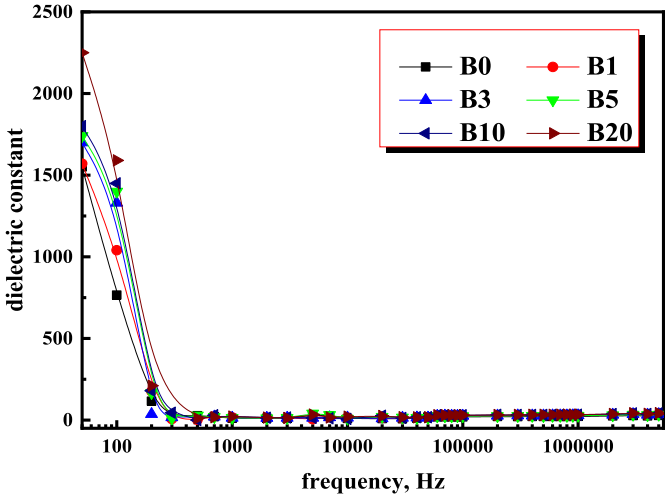

Fig. 8. Variation of dielectric constant for the studied B0 –B20 nanocomposites with the applied frequency at RT.

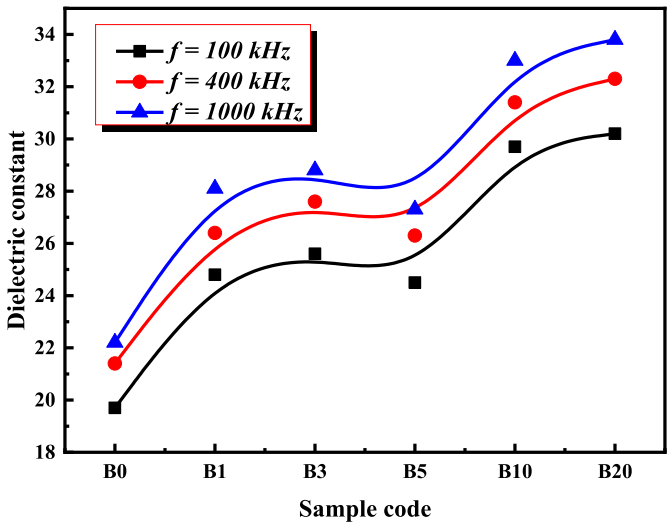

Fig. 9. Variation of dielectric constant with basalt concentration at different frequencies at RT.

the interfacial zone formed around NPs [38,39]. The enhancement in dielectric constant by insertion of basalt NPs can be attributed to the large dielectric constant of basalt compared to pure HDPE.

The fluctuation of the loss tangent, tan δ, of the synthesized B0 – B20 nanocomposites with applied frequency is shown in Fig. 10. For all B0 – B20 nanocomposite samples, the dependence of tan on frequency exhibits roughly the same behavior, with tan values decreasing with increasing frequency during the low-frequency period and becoming semi-constant over the high-frequency interval. The amount of polarization out of alignment is represented by the loss tangent, or tan, which is calculated from the relationship between the dielectric loss and the dielectric constant. Therefore, the observed decrease in tan values of the studied B0 –B20 nanocomposites with an increase in applied frequency could be attributed to the lowering of the charge carriers' tunneling transition [40]. Also, Fig. 10 indicates a sharp increase in tan δ value at frequencies 300 and 4000 Hz. The typical trend has been introduced for high-density polyethylene (HDPE) loaded with zinc and graphite [41, 42]. This sharp increase has been assigned to the interfacial polarization mechanism of heterogeneous systems. Also, Fig. 10 indicates that tan δ values' pronounced dependency on the studied nanocomposites' basalt

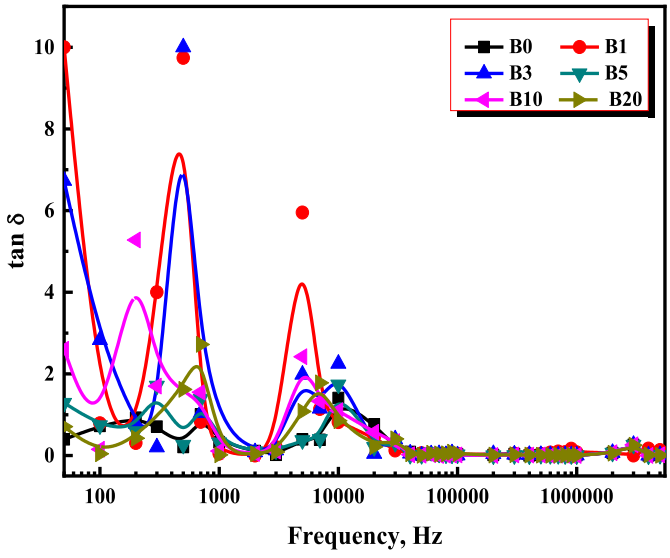

Fig. 10. Variation of tan δ for B0 – B20 nanocomposites with the applied frequency at RT.

concentration does not appear. This can be assigned to competition between two opposite influences due to basalt NPs addition on the conductivity of the created composite: reduction of the mobility of charge carriers in polymer due to trapping of free charges in the interface's zones and the enhancement in density of charge carriers due to inorganic filler [43,44].

4. Conclusion

In the current study, the attenuation parameters of the prepared HDPE doped with basalt powder nano particles increasing from 0.0 to 20.0 wt % with the two radioisotopes Cs-137 and Co-60. Besides, the morphology of the prepared samples, structure, and dielectric properties were also investigated. The μ values were found to be 0.0847–0.1175 cm^{-1}, 0.0571–0.0855 cm^{-1}, 0.0543–0.075 cm^{-1} at 662, 1173, and 1332 keV, for B0– B20, respectively. Also, the HVL was found 12.1366 cm and 12.7530 cm for pure polymer without any modifications at 1173 KeV. These values decreased to be 8.1015 and 9.24 cm for B20 polymer sample. In addition, with increasing the sample thickness and the filler concentration, the RPE was linearly increased. The TF decreased from 92 % to 88 %, 94.44 %–91.8 %, and 94.71 %–92.7 % at 662, 1173, and 1332 keV, respectively. The increase in the TF trend is related to gamma photons' penetration power, that proportional to the photon energy. The FTIR spectra for B0 – B20 samples revealed that four characteristic bands are found without any change in the peak positions at 4000–400 cm^{-1}. besides that, the existence of the filler in the mixture was confirmed by a small shift in the peak positions was noticed as well as a decrease and increase in the peak intensities at 700–400 cm^{-1}. The dielectric constant was enhanced with the enhancement of the filler concentration in the polymer matrix, and this might be due to the large dielectric constant of basalt compared to pure HDPE.

Declaration of competing interest

The authors declare that they have no known competing financial interests or personal relationships that could have appeared to influence the work reported in this paper.

Acknowledgment

The authors would like to thank K. A. Mahmoud (Ural Federal University, Russia and Nuclear Materials Authority, Egypt) and M. A. Abdelkader (Department of Earth Resource Science, Akita University, Japan and Department of Geology, Faculty of Science, Menoufia University, Egypt) for their helping and supporting to achieve this work.

Appendix A. Supplementary data

Supplementary data to this article can be found online at https://doi.org/10.1016/j.net.2023.10.023.

References

[1] Mustafa Recep Kaçal, Hasan Polat, M. Oltulu, Ferdi Akman, O. Agar, H.O. Tekin, Gamma shielding and compressive strength analyses of polyester composites reinforced with zinc: an experiment, theoretical, and simulation-based study, Appl. Phys. A 126 (2020) 1–15.
[2] E. Eren Belgin, G.A. Aycik, A. Kalemtas, A. Pelit, D.A. Dilek, M.T. Kavak, Preparation and characterization of a novel ionizing electromagnetic radiation shielding material: hematite filled polyester based composites, Radiat. Phys. Chem. 115 (2015) 43–48.
[3] I.A. El-Mesady, Y.S. Rammah, A.E. Hussein, H.M. El-Samman, F.I. El-Agawany, R. A. Elsad, Synthesis, optical, mechanical characteristics, and gamma-ray shielding capacity of polyethylene-basalt mixture, Radiat. Phys. Chem. 209 (2023), 110974.
[4] I. El-Mesady, F.I. El-Agawany, H. El-Samman, A. Hussein, Y.S. Rammah, R.A. Elsad, Synthesis, optical characteristics, and gamma-ray protection competence evaluation of polyvinyl chloride reinforced basalt nanocomposites, Radiat. Phys. Chem. (2023), 111122.
[5] O.L. Tashlykov, I.I. Milman, M.W. Aladailah, I.A. Bessonov, S.V. Chalpanov, V. Yu Yarkov, D.O. Pyltsova, E.V. Kuvshinova, K.A. Mahmoud, An extensive experimental study on the role of micro-size pozzolana in enhancing the gamma-ray shielding properties of high-density polyethylene, Radiat. Phys. Chem. (2023), 111079.
[6] Mona M. Gouda, Obeid Amro, Ramadan Awad, Mohamed S. Badawi, Gamma-ray attenuation parameters of HDPE filled with different nano-size and Bulk WO_3, Appl. Radiat. Isot. 197 (2023), 110790.
[7] Guide, Specific Safety, "Radiation Protection and Safety in Medical Uses of Ionizing radiation." Specific Safety Guide SSG-46, IAEA, Vienna, 2018.
[8] Suffian M. Tajudin, F. Tabbakh, Biological polymeric shielding design for an X-ray laboratory using Monte Carlo codes, Radiol. Phys. Technol. 12 (3) (2019) 299–304.
[9] N. Ekinci, K.A. Mahmoud, S. Sarıtaş, B. Aygün, M.M. Hessien, I. Bilici, Y. S. Rammah, Development of Tincal based polypropylene polymeric materials for radiation shielding applications: experimental, theoretical, and Monte Carlo investigations, Mater. Sci. Semicond. Process. 146 (2022), 106696.
[10] Z. Alsayed, M.S. Badawi, R. Awad, A.M. Elkhatib, A.A. Thabet, Investigation of γ-ray attenuation coefficients, effective atomic number and electron density for ZnO/HDPE composite, Phys. Scripta 95 (2022), 085301.
[11] H. Alavian, A. Samie, H. Tavakoli-Anbaran, Experimental and Monte Carlo investigations of gamma-ray transmission and buildup factors for inorganic nanoparticle/epoxy composites, Radiat. Phys. Chem. 174 (2020), 108960.
[12] H.O. Tekin, F. Akman, S.A. Issa, M.R. Kaçal, O. Kilicoglu, H. Polat, Two-step investigation on fabrication and characterization of iron-reinforced novel composite materials for nuclear-radiation shielding applications, J. Phys. Chem. Solid. 146 (2020), 109604.
[13] S.A.M. Issa, A.M.A. Mostafa, T.A. Hanafy, M. Dong, X. Xue, Comparison study of photon attenuation characteristics of Polyvinyl alcohol (PVA) doped with Pb $(NO_3)_2$ by MCNP5 code, XCOM, and experimental results, Prog. Nucl. Energy 111 (2019) 15–23.
[14] O. Kilicoglu, C.V. More, F. Akman, K. Dilsiz, H. Oğul, M.R. Kaçal, H. Polat, O. Agar, Micro Pb filled polymer composites: theoretical, experimental and simulation results for γ ray shielding performance, Radiat. Phys. Chem. 194 (2022), 110039.
[15] I. Bilici, B. Aygün, C.U. Deniz, B. Öz, M.I. Sayyed, A. Karabulut, Fabrication of novel neutron shielding materials: polypropylene composites containing colemanite, tincal and ulexite, Prog. Nucl. Energy 141 (2021), 103954.
[16] E. Ekinci, K.A. Mahmoud, B. Aygün, M.M. Hessien, Y.S. Rammah, Impacts of the colemanite on the enhancement of the radiation shielding capacity of polypropylene, J. Mater. Sci. Mater. Electron. 33 (25) (2022) 20046–20055.
[17] El-Khatib, M. Ahmed, Mona M. Gouda, Mohamed S. Fouad, Mohamed Abd-Elzaher, Wegdan Ramadan, Radiation attenuation properties of chemically prepared MgO nanoparticles/HDPE composites, Sci. Rep. 13 (1) (2023) 9945.
[18] F. Akman, H. Ogul, I. Ozkan, Mustafa Recep Kaçal, O. Agar, Hasan Polat, Kamuran Dilsiz, Study on gamma radiation attenuation and non-ionizing shielding effectiveness of niobium-reinforced novel polymer composite, Nucl. Eng. Technol. 54 (1) (2022) 283–292.
[19] Elhassan A. Allam, Rehab M. El- Sharkawy, Atef El-Taher, E.R. Shaaban, E. El Sayed Massoud, Mohamed E. Mahmoud, Enhancement and optimization of gamma radiation shielding by doped nano HgO into nanoscale bentonite, Nucl. Eng. Technol. 54 (6) (2022) 2253–2261.
[20] Tom Anto, C.R. Rejeesh, Synthesis and characterization of recycled HDPE polymer composite reinforced with nano-alumina particles, Mater. Today: Proc. 72 (2023) 3177–3182.
[21] H.M. Eyssa, Rawia F. Sadek, Wael S. Mohamed, Wageeh Ramadan, Structure property behavior of polyethylene nanocomposites containing Bi_2O_3 and WO_3 as an ecofriendly additive for radiation shielding, Ceram. Int. 49 (11) (2023), 1844218454.
[22] Xiang Gou, Xuan Zhao, Surjit Singh, Da Qiao, Tri-pyrolysis: a thermo-kinetic characterization of polyethylene, cornstalk, and anthracite coal using TGA-FTIR analysis, Fuel 252 (2019) 393–402.
[23] Xingping Kai, Rundong Li, Tianhua Yang, Shengqiang Shen, Qiuxia Ji, Tao Zhang, Study on the co-pyrolysis of rice straw and high-density polyethylene blends using TGFTIR-MS, Energy Convers. Manag. 146 (2017) 20–33.
[24] Alok K. Sahu, K. Sudhakar, R.M. Sarviya, Influence of UV light on the thermal properties of HDPE/Carbon black composites, Case Stud. Therm. Eng. 15 (2019), 100534.
[25] S.M. Khan, N. Gull, M.A. Munawar, A. Islam, S. Zia, M. Shafiq, A. Sabir, S. M. Awais, M.A. Butt, M.T.Z. Butt, T. Jamil, 2D carbon fiber reinforced high-density polyethylene multi-layered laminated composite panels: structural, mechanical, thermal, and morphological profile, J. Mater. Sci. Technol. 32 (10) (2016) 1077–1082.
[26] J.V. Gulmine, P.R. Janissek, H.M. Heise, L. Akcelrud, Polyethylene characterization by FTIR, Polym. Test. 21 (5) (2002) 557–563.
[27] Ş. Erdem, F. Özgür, B. Alim, M.I. Sayyed, M. Kurudirek, Phy-X/PSD: development of a user-friendly online software for calculation of parameters relevant to radiation shielding and dosimetry, Radiat. Phys. Chem. 166 (2020), 108496.
[28] E. Atta, K.M. Zakaria, A. Madbouly, Research article study on polymer clay layered nanocomposites as shielding materials for ionizing radiation, Int J Recent Sci Res 6 (5) (2015) 4263–4269.
[29] A. Sharma, M.I. Sayyed, O. Agar, M.R. Kacal, H. Polat, F. Akman, Photon-shielding performance of bismuth oxychloride-filled polyester concretes, Mater. Chem. Phys. 241 (2020), 122330.
[30] M.E. Mahmoud, A.M. El-Khatib, M.S. Badawi, A.R. Rashad, R.M. El-Sharkawy, A. A. Thabet, Fabrication, characterization and gamma rays shielding properties of nano and micro lead oxide dispersed- high density polyethylene composites, Radiat. Phys. Chem. 145 (2018) 160–173.
[31] M.E. Mahmoud, A.M. El-Khatib, M.S. Badawi, A.R. Rashad, R.M. El-Sharkawy, A. A. Thabet, Recycled high-density polyethylene plastics added with lead oxide

nanoparticles as sustainable radiation shielding materials, J. Clean. Prod. 176 (2018) 276–287.
[32] F. Akman, M.R. Kacal, N. Almousa, M.I. Sayyed, H. Polat, Gamma ray attenuation parameters for polymer composites reinforced with $BaTiO_3$ and $CaWO_4$ compounds, Prog. Nucl. Energy 121 (2020), 103257.
[33] R. Li, Y. Gu, Y. Wang, Z. Yang, M. Li, Z. Zhang, Effect of particle size on gamma radiation shielding property of gadolinium oxide dispersed epoxy resin matrix composite, Mater. Res. Express 4 (3) (2017), 035035.
[34] A.E.-S. Abdo, M. Ali, M. Ismail, Natural fiber high-density polyethylene and lead oxide composites for radiation shielding, Radiat. Phys. Chem. 66 (3) (2003) 185–195.
[35] S.F.A. Ali, R.A. Elsad, S.A. Mansour, " Enhancing the dielectric properties of compatibilized high-density polyethylene/calcium carbonate nanocomposites using high density polyethylene-g-maleic anhydride", Polym. Bull. 10 (2020) 1–13.
[36] S.A. Mansour, I.S. Yahia, G.B. Sakr, Electrical conductivity and dielectric relaxation behavior of fluorescein sodium salt (FSS), Solid State Commun. 150 (2010) 1386–1391.
[37] S.A. Mansour, I.S. Yahia, F. Yakuphanoglu, The electrical conductivity and dielectric properties of CI Basic Violet 10, Dyes Pigments 87 (2010) 144–148.
[38] R.A. Elsad, K.A. Mahmoud, Y.S. Rammah, A.S. Abouhaswa, Fabrication, structural, optical, and dielectric properties of PVC-PbO nanocomposites" as well as their gamma-ray shielding capability, Radiat. Phys. Chem. 189 (2021), 109753.
[39] O.F. El-Menshawy, A.R. El-Sissy, M.S. El-Wazery, R.A. Elsad, Electrical and mechanical performance of hybrid and non-hybrid composites, Int. J. Eng. 32 (2019), 580586.
[40] S. Singha, M.J. Thomas, Influence of filler loading on dielectric properties of Epoxy ZnO nanocomposites, IEEE Trans. Dielectr. Electr. Insul. 16 (2009) 531–542.
[41] V. Panwar, R.M. Mehra, Analysis of electrical, dielectric, and electromagnetic interference shielding behaviour of graphite filled high-density polyethylene composites, Polym. Eng. Sci. 10 (1) (2008) 2178–2187.
[42] S.A. Mansour, R.A. Elsad, M.A. Izzularab, " Dielectric investigation of high-density polyethylene loaded by ZnO nanoparticles synthesized by sol–gel route", J. Sol. Gel Sci. Technol. 80 (2) (2016) 333–341.
[43] S.A. Mansour, R.A. Elsad, M.A. Izzularab, Dielectric properties enhancement of PVC nano dielectrics based on synthesized ZnO nanoparticles, J. Polym. Res. 23 (5) (2016) 978–985, 23(5):978–985.
[44] S.A. Mansour, R.A. Elsad, M.A. Izzularab, Dielectric spectroscopic analysis of polyvinyl chloride nanocomposites loaded with Fe_2O_3 nano crystals, Polym. Adv. Technol. 29 (9) (2018) 2477–2485.